ELSEVIER

Advances in Colloid and Interface Science
76–77 (1998) 203–226

ADVANCES IN COLLOID AND INTERFACE SCIENCE

Density functional theory model for calculating pore size distributions: pore structure of nanoporous catalysts

Peter I. Ravikovitch[a], Gary L. Haller[a], Alexander V. Neimark[a,b,*]

[a] *Chemical Engineering Department, Yale University, New Haven, CT 06520-8286, USA*
[b] *TRI / Princeton, Princeton, NJ 08542-0625, USA*

Abstract

Using the example of nanoporous catalysts, we discuss the non-local density functional theory (NLDFT) model applied to physical adsorption of nitrogen and argon. The model has been used for predicting adsorption/desorption isotherms in nanopores of different geometries over a wide range of pore sizes (0.5–100 nm), and for calculating pore size distributions from adsorption isotherms based on given intermolecular fluid–fluid and fluid–solid potentials. The development of new nanoporous catalysts requires reliable characterization methods. We critically analyze different methods which are currently used for pore structure characterization in the range of nanometers. Calculations of the pore size distributions from nitrogen and argon adsorption isotherms are presented. Our primary method is based on the NLDFT model of adsorption on MCM-41, developed earlier. The results obtained with the NLDFT model are compared with other methods. It is shown, that the pore structure of nanoporous catalysts can be quite complex, and that Ar and N_2 isotherms contain complimentary information. The NLDFT model is recommended for evaluation of pore size distributions in nanoporous catalysts and other MCM-41 based materials.

Keywords: Adsorption; Density functional theory; Pore size distribution; Nanoporous catalysts; MCM-41

* Corresponding author. E-mail: aneimark@triprinceton.org

PII S0001-8686(98)00047-5

Contents

1. Introduction

Recent advances in the synthesis of uniform nanoporous materials with controlled pore size in the range of 2–10 nm present new possibilities for the applications of these materials in catalysis. Recently, a family of the mesoporous molecular sieves, designated M41S, has been discovered by Mobil scientists (Kresge et al. [1], Beck et al. [2]). One of the members of this family, MCM-41, possesses an array of uniform channels arranged on a two-dimensional hexagonal lattice. Other members of this family have cubic (MCM-48) and lamellar (MCM-50) structures [1–5]. Materials similar to MCM-41 include FSM-16 derived from kanemite [6,7] and HMS materials [8,9]. Other organic–inorganic mesophases have also been synthesized, e.g. SBA-2 with a three-dimensional hexagonal structure [10]. Desired catalytic properties of new periodic mesoporous materials can be achieved by incorporation of foreign ions into the siliceous MCM-41 structure which will constitute catalytic sites, e.g. Al and Ga as acid sites or Ti and V as oxidation sites. Synthesis of aluminosilicates [1,2,11–13], titanosilicates [14–17], incorporation of V [18], Cr [19] and other metals have been reported. More references on the synthesis, characterization, and potential applications of M41S and related materials and catalysts can be found in recent reviews [20,21].

In this work, we focus on the physical adsorption as a method for characterization of the pore structure of M41S materials, in particular, on the calculations of pore size distributions from the density functional theory molecular model of adsorption on MCM-41 recently proposed [22,23]. The paper is organized as follows. In Section 2 we give a brief description of the methods used for the characterization of M41S and related materials. In Section 3, we focus on the phenomenological approaches proposed for the interpretation of adsorption isotherms and calculating the pore structure parameters of MCM-41 materials. In Section 4, we give the description of the non-local density functional theory (NLDFT) model for nitrogen and argon adsorption on MCM-41, and the method for calculating the pore size distributions in MCM-41 materials based on the NLDFT model. In Section 5, we give examples of the pore size distribution calculations in MCM-41 catalysts and compare our results with some other

methods. In Conclusions, we give some recommendations regarding the use of different methods for interpretation of physisorption isotherms in nanoporous materials and calculating the pore size distributions.

2. Methods for characterization of M41S materials

The three most widely used methods of characterization of MCM-41 material are: (1) X-ray diffraction data (XRD), (2) transmission electron microscopy (TEM), and (3) physical adsorption. These methods have been used in the vast majority of publications on characterization of MCM-41 and related materials and catalysts. A critical appraisal of these methods has been given by Ciesla et al. [24]. Here, we mention briefly the main advantages and drawbacks of each of these methods.

X-Ray diffraction is used as a primary source of information on the structure of M41S and related materials. The characteristic XRD patterns of the hexagonal, cubic and lamellar mesophases found in M41S and related materials are well documented [1–5,10,21]. The XRD pattern of the ideal hexagonal structure of MCM-41 exhibits four characteristic peaks (100, 110, 200 and 210). However, for many samples, especially after incorporation of transition metals, XRD patterns show only a single peak. A single XRD peak cannot be indexed for certain [24]. On the other hand, low-temperature nitrogen and argon adsorption isotherms on such samples often exhibit relatively sharp capillary condensation steps, characteristic of adsorption on MCM-41 materials, which points toward a fairly uniform pore size distribution. Even when diffraction data indicate a well ordered structure, it is difficult to quantify the purity of the material [24]. The main weakness of the XRD analysis is that it does not provide direct information about the *internal pore size* and the thickness of pore walls which are relevant parameters from the viewpoint of catalytic applications. Thus, XRD measurements should be combined with other methods.

Transmission electron microscopy provides a direct picture of the material, and usually, with quite high resolution. In principle, the periodicity of pore channels, their internal diameter, and the pore wall thickness can be directly measured, and even some information about the length of pore channels can be obtained. Some problems arise due to defocusing in the TEM measurements. Chen et al. [7] illustrated this point by plotting the variations in the determined pore wall thickness versus various amounts of defocus. By extrapolating to zero defocus, the pore wall thickness of hexagonal material derived from kanemite was found to be 0.7 nm [7]. This value is in agreement with the data of Monnier et al. [3] who estimated the pore wall thickness of the hexagonal mesophase of approximately 0.8–0.9 nm, based on the volumetric considerations and X-ray data. Similar values have been recently reported by Inagaki et al. [25] for the hexagonal material derived from kanemite. Molecular dynamics simulations of the structure of MCM-41 with a lattice constant of approximately 4.5–5 nm, performed using an amorphous silica model, showed that the simulated XRD patterns for the pore wall thickness $\geq$ 1 nm are in excellent agreement with the experimental data [26].

In the TEM measurements, only a small fraction of material can be seen, leaving the statistical uncertainty of the results an open question. It has been shown, that even in high-quality MCM-41 materials, very different regions can be seen in the TEM pictures [24]. Thus, in order to obtain reliable information, a representative fraction of the material has to be analyzed.

In contrast to TEM, physical adsorption isotherms have the advantage of producing a macroscopic average measurement, from which such characteristics as the specific surface area, the pore volume, and the pore size distribution (PSD) are obtained [27]. Adsorption isotherms are also very sensitive to peculiarities of the pore structure which manifest themselves in the shape of the adsorption isotherms. By combining the adsorption measurements with the XRD data, one can obtain the minimal value for the pore wall thickness. However, the interpretation of adsorption isotherms and calculation of the pore structure parameters require the use of adsorption models. The *quantitative* interpretation of the adsorption isotherms is complicated because the typical pore size of M41S materials is only approximately 7–13 molecular diameters of the adsorbate molecule, and assumptions made in the traditional models such as Brunauer-Emmett-Teller (BET) [27] and Barrett-Joyner-Halenda (BJH) [28] become much less realistic. Thus, development of new approaches and models is topical for the characterization of nanoporous materials. In the next section we give a short description of the methods currently used for the characterization of MCM-41 materials from low-temperature adsorption isotherms.

3. Methods proposed for characterization of MCM-41 materials from adsorption isotherms

Physical adsorption was widely used for characterization of MCM-41 materials [1,2,22,23,29–44]. The common and the most distinctive feature of sub-critical adsorption isotherms on MCM-41 is a characteristic step associated with the capillary condensation in pore channels. It has been shown that, depending on adsorbate, pore size and temperature, the capillary condensation/desorption in MCM-41 may proceed both with and without hysteresis [22,23,29,32–35,37,40,43]. At 77 K, nitrogen adsorption isotherms are reversible for MCM-41 samples with pore size smaller than approximately 4–4.2 nm, i.e. for most of the presently synthesized samples. However, hysteresis of argon isotherms at 77 K is observed for MCM-41 when the pore size is greater than approximately 3.3–3.5 nm, and at 87 K, the Ar hysteresis is observed for pore sizes greater than approximately 3.7–4 nm [40]. Also, the nitrogen isotherm on a 4.3–4.5 nm MCM-41 exhibits a well defined hysteresis at lower temperature, i.e. 71 K [22,23]. The behavior of the hysteresis loops in cylindrical pores is explained on the basis of the results of density functional theory [22,23]. According to the DFT model, the fluid in pores is undergoing a phase transition, accompanied by metastable states. The model predicts the adsorption/desorption isotherms and the limits of the *thermodynamic*

hysteresis loop (spinodal points), and the equilibrium transition pressure [22,23,29]. The model is described in the next section.

One of the commonly used methods for calculating the pore diameter in MCM-41 materials is based on the following relation [33]:

$$D_{4V/S} = \frac{4V_p}{S_{total} - S_{ext}} \quad (1)$$

where V_p is the volume of mesopores, S_{total} is the total surface area, and S_{ext} is the external surface area. The volume of mesopores is usually calculated by converting the amount adsorbed right after the capillary condensation step into liquid volume, using the density of the bulk liquid nitrogen. The total surface area is calculated either from the BET method or from the *t*-plot, comparison, or α–S plots [27]. The external surface area is also calculated from the comparison plot in the region of relative pressures above the step. Sometimes, the volume of mesopores is also calculated from the comparison plot at high pressures. Standard isotherms on non-porous silicas are usually employed to construct the comparison plots. While the relation (1) is widely used for calculating an average pore size of MCM-41 [33,39], it should be noted that the density of the adsorbate in small cylindrical pores may differ from the density of the bulk liquid, and that determined surface areas may also be in error. The external surface areas are especially inaccurate because the comparison plots at high relative pressures are often non-linear and thus, the regression line is to some degree arbitrary.

The foundation for this approach comes from the observation that in most cases, comparison or α–S plots for nitrogen [30–33,43], argon [30,32,43] carbon dioxide [36], and cyclopentane [31,35] adsorption isotherms on MCM-41 are linear and can be back-extrapolated to the origin. This confirms the absence of micropores, and points toward similarity of the chemical structure of the pore walls of MCM-41 and silica. The surface areas determined from the comparison plots are close to those calculated from the BET method, which merely reflects the fact that the surface areas of the reference isotherms are usually determined from the BET method. Ravikovitch et al. [43] constructed nitrogen and argon low-pressure comparison plots versus isotherms on a well-characterized high-purity reference MCM-41 material with a wide pore size of approximately 4.3–4.5 nm [22]. It has been shown that comparison plots for pure siliceous and V substituted MCM-41-like materials remained linear even for the samples with the smallest pore size, i.e. those prepared from C8 and C10 surfactants [43]. It should be noted that the BET method is inapplicable to isotherms on materials with such small pores. In small pore samples, the upward deviations of the comparison plots associated with the pore filling occur at relative pressure of approximately $P/P_0 \approx 0.03$, which is usually the lower limit of the linearity of the BET plots. The inaccuracy of the BET method for small pore materials has also been noted by Kruk et al. [42].

The pore size of high-quality MCM-41 materials can also be calculated based on purely geometrical considerations. Considering an infinite hexagonal array of

cylindrical pores, with a known length of a unit cell, the density of the pore wall material, and the pore volume, then the pore diameter can be calculated [13,41,42].

The BJH method [28] is the standard procedure for calculating the pore size distribution in mesoporous materials. The essence of the BJH method is the modified Kelvin equation. The radius of the capillary appearing in the Kelvin equation is replaced by the pore radius minus the thickness of the adsorbed film. The thickness of the adsorbed film is taken from the standard *t*-curve on a non-porous surface [27]. The modified Kelvin equation is widely used for calculating the pore size distributions in MCM-41 materials [32,37]. It has been shown that the modified Kelvin equation underestimates the pore size in the range of nanopores, and consequently, overestimates the pore wall thickness obtained by subtracting the adsorption pore size from the XRD data [22,43]. The thickest pore wall thickness in MCM-41 materials obtained by the BJH method was reported to be 26.8 Å [45], which seems to be unrealistically large.

Naono et al. [44] have proposed to derive the thickness of the adsorbed layer to be used in the modified Kelvin equation from the experimental isotherms. From the comparison plot, the volume of mesopores, total and external surface areas, and the volume of the layer at the point of the capillary condensation are derived. The thickness of the adsorbate film is then calculated from a geometrical relation. Using experimental nitrogen isotherms on a series of FSM-16 samples with different pore sizes, the authors have derived the thickness of the adsorbed layer at the points of the capillary condensation for pores of different sizes [44].

The Horvath-Kawazoe (HK) method [46] is also often used to obtain the pore size of MCM-41 materials [2,9,47]. It should be noted that the HK method was originally developed for calculating pore size distributions in microporous carbons using the slit pore model. The method was extended to the cylindrical pore model by Saito and Foley [48] who developed this model for calculating the pore size distributions in zeolites [49]. In the HK approach, the average potential field inside the pore is related to the change in the free energy during adsorption, yielding a relation between the pore size and the relative pressure at which the pore fills with the adsorbate. The applicability of this method for calculating the pore size distribution of MCM-41 is doubtful, and may even lead to misleading results [50].

4. The non-local density functional theory model of adsorption on MCM-41

Molecular models of adsorption such as density functional theory (DFT) and Monte Carlo (MC) simulations give a much more accurate description of adsorption phenomena [51]. Based on given intermolecular potentials of fluid–fluid and fluid–solid interactions, they allow the construction of adsorption isotherms in model pores. Methods for characterization of porous solids based on the rigorous statistical mechanical approaches are being developed. The main focus has been placed on the calculation of pore size and adsorption energy distributions in microporous carbons [52–59]. MC simulations of adsorption on MCM-41 were performed by Maddox and coworkers [60,61]. We have developed the non-local

density functional theory (NLDFT) model of adsorption on MCM-41 [22,23,29,40,43].

Density functional theory is a powerful method for description of inhomogeneous fluids. The basic formulations of the DFT approach can be found in [62,63]; for a review see Evans [64]. DFT methods were employed in numerous studies related to vapor–liquid equilibrium, wetting and layering transitions, structure of simple fluids in pores, single component and binary mixture adsorption in model pores [65–94], and the calculation of the pore size distributions from adsorption isotherms [22,23,40,43,52–57]. The non-local density functional theory (NLDFT) model of adsorption on MCM-41 is based on the density functional developed by Tarazona and coworkers [69,73], and is known as the Smoothed Density Approximation (SDA). This version of the theory was used effectively for studying adsorption in model pores [75,76,81,83–88,90–94] and for calculating the pore size distributions in carbons [54–57].

In the DFT approach, the local fluid density $\rho(\mathbf{r})$ of the adsorbate confined in a pore at given chemical potential μ and temperature T is determined by minimization of the grand thermodynamic potential (GP). The GP is expressed as a function of the fluid density $\rho(\mathbf{r})$:

$$\Omega[\,\rho(\mathbf{r})] = F[\,\rho(\mathbf{r})] - \int \mathrm{d}\mathbf{r}\rho(\mathbf{r})[\,\mu - U_{\mathrm{ext}}(\mathbf{r})] \tag{2}$$

where $F[\,\rho(\mathbf{r})]$ is the intrinsic Helmholtz free energy functional, and $U_{\mathrm{ext}}(\mathbf{r})$ is the potential imposed by the pore walls. In a perturbation fashion, the Helmholtz free energy is divided into the contribution from the reference system of hard spheres, and the contribution from attractive interactions. The attractive term is treated in a mean-field approximation:

$$F[\,\rho(\mathbf{r})] = \int \mathrm{d}\mathbf{r}\rho(\mathbf{r})\left[k_{\mathrm{B}}T(\ln(\Lambda^3\rho(\mathbf{r})) - 1) + f_{\mathrm{ex}}[\,\bar{\rho}(\mathbf{r});d_{\mathrm{HS}}]\right] + \frac{1}{2}\int\int \mathrm{d}\mathbf{r}\,\mathrm{d}\mathbf{r}'\rho(\mathbf{r})\rho(\mathbf{r}')\Phi_{\mathrm{attr}}(|\mathbf{r}-\mathbf{r}'|) \tag{3}$$

where $\Phi_{\mathrm{attr}}(r)$ is the attractive potential; Λ denotes the de Broglie thermal wavelength in the ideal gas term; $f_{\mathrm{ex}}[\,\bar{\rho}(\mathbf{r});d_{\mathrm{HS}}]$ is the excess free energy per molecule in the hard sphere fluid, which is calculated from the Carnahan-Starling equation of state [95]. The SDA implies that $f_{\mathrm{ex}}[\,\bar{\rho}(\mathbf{r});d_{\mathrm{HS}}]$ depends on the smoothed density $\bar{\rho}(\mathbf{r})$ defined as

$$\bar{\rho}(\mathbf{r}) = \int \mathrm{d}\mathbf{r}'\rho(\mathbf{r}')\,\omega(|\mathbf{r}-\mathbf{r}'|,\bar{\rho}(\mathbf{r})) \tag{4}$$

where the weighting function $\omega(|\mathbf{r}-\mathbf{r}'|)$ was chosen to reproduce the Percus-Yevick approximation for the direct correlation function of the homogeneous hard-sphere fluid [69,73].

Table 1
Parameters of the NLDFT model for N_2 and Ar adsorption on MCM-41

Adsorbate	ϵ_{ff}/k_B (K)	σ_{ff} (Å)	d_{HS} (Å)	r_c (Å)	$\rho_S\ \epsilon_{sf}/k_B$ (K/Å^2)	σ_{sf} (Å)
N_2	94.45	3.575	3.575	$5\sigma_{ff}$	22.53	3.17
Ar	118.05	3.305	3.38	$5\sigma_{ff}$	26.2	3.0

ρ_s, surface number density.

The attractive interactions are modeled with the Lennard-Jones potential, split according to the WCA perturbation scheme [96] in its minimum, at $r_m = 2^{1/6}\sigma_{ff}$:

$$\Phi_{attr}(r) = \begin{cases} -\epsilon_{ff}, & r < r_m \\ 4\epsilon_{ff}\left[(\sigma_{ff}/r)^{12} - (\sigma_{ff}/r)^{6}\right], & r_m < r < r_c \\ 0, & r > r_c \end{cases} \tag{5}$$

where r_c is a cutoff distance.

The minimization of the Grand Potential by the method of Indeterminate Lagrange Multipliers (ILM) yields the following equation for the density profile $\rho(\mathbf{r})$ [97]:

$$\mu = k_B T \ln(\rho(\mathbf{r})\Lambda^3) + f_{ex}[\bar{\rho}(\mathbf{r}); d_{HS}] - \int d\mathbf{r}'\lambda(\mathbf{r}')\omega(|\mathbf{r} - \mathbf{r}'|, \bar{\rho}(\mathbf{r}')) + U_{ext}(\mathbf{r}) + \int d\mathbf{r}'\rho(\mathbf{r}')\Phi_{attr}(|\mathbf{r} - \mathbf{r}'|) \tag{6}$$

with the ILM function:

$$\lambda(\mathbf{r}) = -\rho(\mathbf{r}) f_{ex}'(\mathbf{r}) \Big/ \left[1 - \int d\mathbf{r}'\rho(\mathbf{r}')\frac{d\,\omega(|\mathbf{r} - \mathbf{r}'|, \bar{\rho}(\mathbf{r}))}{d\,\bar{\rho}(\mathbf{r})}\right] \tag{7}$$

The bulk fluid of a uniform density, ρ, is described by the following equations of state:

$$\mu(\rho) = \mu_H(\rho) + \rho \int d\mathbf{r}\Phi_{attr}(|\mathbf{r}|) \tag{8a}$$

$$P(\rho) = P_H(\rho) + \tfrac{1}{2}\rho^2 \int d\mathbf{r}\Phi_{attr}(|\mathbf{r}|) \tag{8b}$$

where $\mu_H(\rho)$ and $P_H(\rho)$ are the chemical potential and the pressure of the hard sphere fluid, respectively.

Parameters of the LJ fluid–fluid potentials (ϵ_{ff}, σ_{ff}) are listed in Table 1. NLDFT involves an additional parameter, the equivalent hard sphere diameter,

d_{HS}, which is not supposed to be necessarily equal to σ_{ff}, and serves as an adjustable parameter to provide the best fit to the experimental bulk fluid properties. The parameters of the fluid–fluid interactions for N_2 and Ar were fitted such that the theory provides a good fit to the experimental *liquid–gas coexistence densities*, *saturation pressure*, and the *surface tension* of the free liquid–gas interface [22,40]. Correct prediction of the surface tension is a necessary condition for any model used for the quantitative description of the capillary condensation/desorption transitions in pores. The liquid–gas coexistence densities and saturation pressure of bulk N_2 at 77 K are predicted with an accuracy better than 1%, and the surface tension is only 1.5% greater than the experimental value of 8.88 mN/m [40]. For Ar, the equilibrium liquid–gas densities agree to within 1% with the experimental data in the temperature range from 83 to 90 K, and within 5% at temperatures up to 105 K. The saturation pressure is predicted with an accuracy better than 2% for up to 125 K. The surface tension of Ar is predicted with an accuracy better than 2% in the temperature range from 83 to 90 K, and with up to 5% at temperatures up to 110 K [40].

The solid–fluid interactions are modeled with the LJ potential integrated over the cylindrical surface and accounting for the pore curvature [98]:

$$U_{ext}(r,R) = \pi^2 \rho_s \epsilon_{sf} \sigma_{sf}^2 \left[\frac{63}{32} \left[\frac{r}{\sigma_{sf}} \left(2 - \frac{r}{R} \right) \right]^{-10} F\left[-\frac{9}{2}, -\frac{9}{2}; 1; \left(1 - \frac{r}{R} \right)^2 \right] \right.$$
$$\left. - 3 \left[\frac{r}{\sigma_{sf}} \left(2 - \frac{r}{R} \right) \right]^{-4} F\left[-\frac{3}{2}, -\frac{3}{2}; 1; \left(1 - \frac{r}{R} \right)^2 \right] \right] \tag{9}$$

with $F[\alpha,\beta,\gamma,\chi]$ being the hypergeometric series, and ρ_s is the density of oxygen atoms in the pore wall. For an infinitely large pore radius this potential reduces to the $10 - 4$ potential.

In this model, the fluid density is considered a function of the radial coordinate r. For a given chemical potential, μ, Eqs. (6),(7) are solved for the density profile, $\rho(r)$. The excess adsorption isotherm per unit of pore volume is calculated as

$$N_V(\mu) = \frac{8}{(D - \sigma_{ss})^2} \int_0^{D/2 - \sigma_{ss}} r \, dr \left[\rho(r) - \rho_g(\mu) \right] \tag{10}$$

where ρ_g is the bulk gas density, and $\sigma_{ss} = 2.76$ Å is the effective diameter of oxygen atoms in the pore wall. Here, adsorption is defined as an excess quantity with respect to the equilibrium density in the bulk, and the reference fluid volume is defined as the internal (geometrical) volume of the pore with $D_{in} = D - \sigma_{ss}$. A rigorous approach for calculating the excess adsorption is discussed in [94].

The parameters of the solid–fluid potential (Eq. (9)) were chosen to fit the N_2 and Ar standard isotherms on nonporous siliceous materials in the multilayer adsorption region. In Fig. 1, we present a comparison of the NLDFT isotherm in a slit pore of width $H_{in} = 53.3$ nm with the standard isotherm of nitrogen on

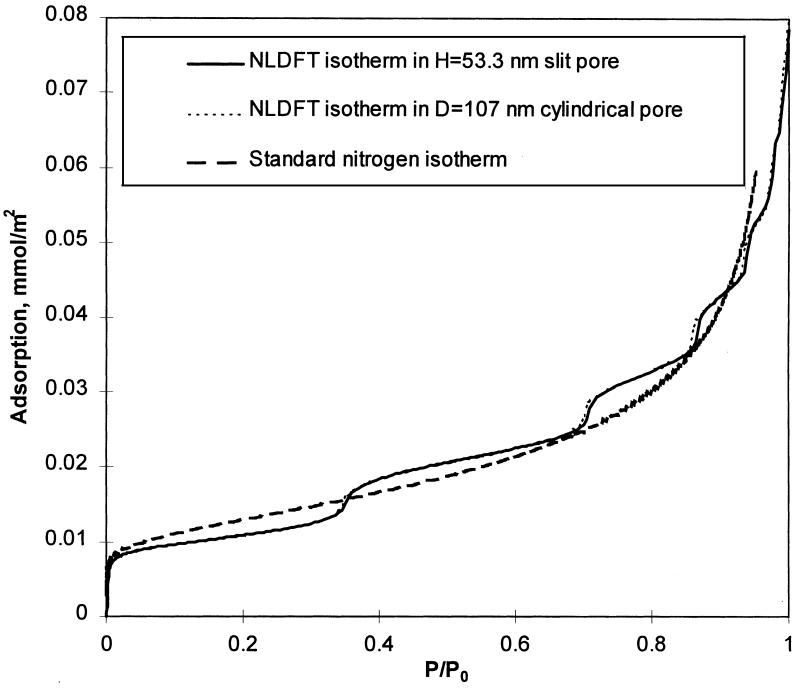

Fig. 1. Comparison of the NLDFT adsorption isotherms of N_2 at 77 K in the slit pore of 53.3 nm in diameter and the cylindrical pore of 107 nm in diameter with the reference isotherm of de Boer et al. [99]. The equilibrium capillary condensation transition occurs at $P/P_0 = 0.978$ (not shown).

non-porous oxides as given by de Boer et al. [99] and Dubinin et al. [100]. The simplified treatment of the solid–fluid interactions using the homogeneous potential does not allow for a detailed description of the isotherm in the monolayer region and prediction of a smooth multilayer adsorption isotherm. However, the overall shape of the multilayer adsorption isotherm is represented quite well (Fig. 1). According to the Kelvin equation, the equilibrium capillary condensation pressure in a cylindrical pore of diameter D is the same as in a slit pore of width $D/2$. One should expect this property to be valid for the NLDFT predictions in the limit of large pores. To check this, we have performed calculations for the cylindrical pore of size $D_{in} = 107$ nm $\approx 2H_{in}$. The two isotherms expressed per unit of pore area are practically identical (Fig. 1). The equilibrium capillary condensation transition occurs at the relative pressure $P/P_0 = 0.978 \pm 0.001$, both for the slit and the cylindrical pores. However, the Kelvin equation predicts $P/P_0 = 0.982$, which is related to a pore of approximately 20% wider.

Note, that the solid–fluid interaction parameters used in this paper differ somewhat from the parameters which we used in previous calculations of nitrogen adsorption on MCM-41 [22,23,40,43]. The updated parameters were chosen to provide a better agreement with the reference adsorption isotherm (Fig. 1).

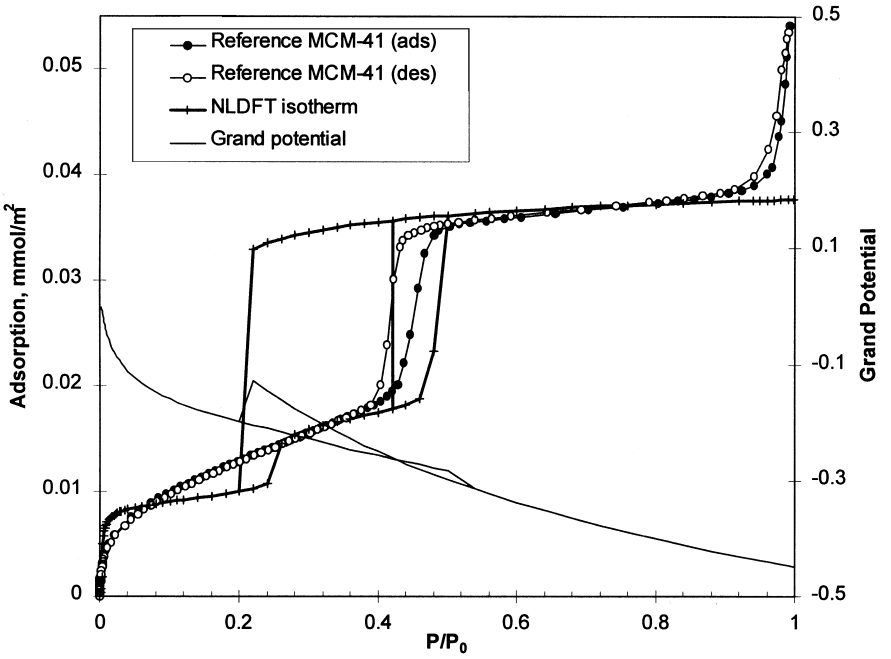

Fig. 2. Comparison of the NLDFT isotherm of Ar at 87 K in the cylindrical pore of 4.36 nm in diameter with the experimental isotherm on a reference MCM-41 sample [22] Changes in the grand potential are shown by a thin solid line (after [29]).

In Fig. 2, we present as a typical example [29], the calculated isotherm of Ar at 87 K in the cylindrical pore of 4.36 nm (internal diameter) in comparison with the isotherm on a reference MCM-41 sample with the pore size of approximately 4.4 nm [22]. The theoretical isotherm exhibits metastable adsorption and desorption branches of the hysteresis loop, which are tracing the equilibrium state characterized by smaller values of the grand potential. The equilibrium thermodynamic transition may occur between the states of equal grand potential. Thus, the intersection of the grand potential adsorption and desorption isotherms corresponds to the point of the equilibrium transition, which is indicated by a vertical line. Comparison with the experimental hysteresis loop clearly shows that the experimental desorption branch is very close to the equilibrium transition, while the experimental adsorption branch is placed within the loop formed by the metastable theoretical adsorption isotherm and the equilibrium transition line. Many other similar examples of N_2 isotherms at 77 K and at 70.6 K, and Ar at 77 K and at 87 K on the reference MCM-41 samples have been reported in [22,23,29,40].

The experimentally observed transition is smoothed in comparison with the theoretical prediction for a single pore because of some degree of pore size heterogeneity which is present even in 'ideal' MCM-41. However, on the basis of comparison of the NLDFT calculated isotherms and the experimental isotherms on

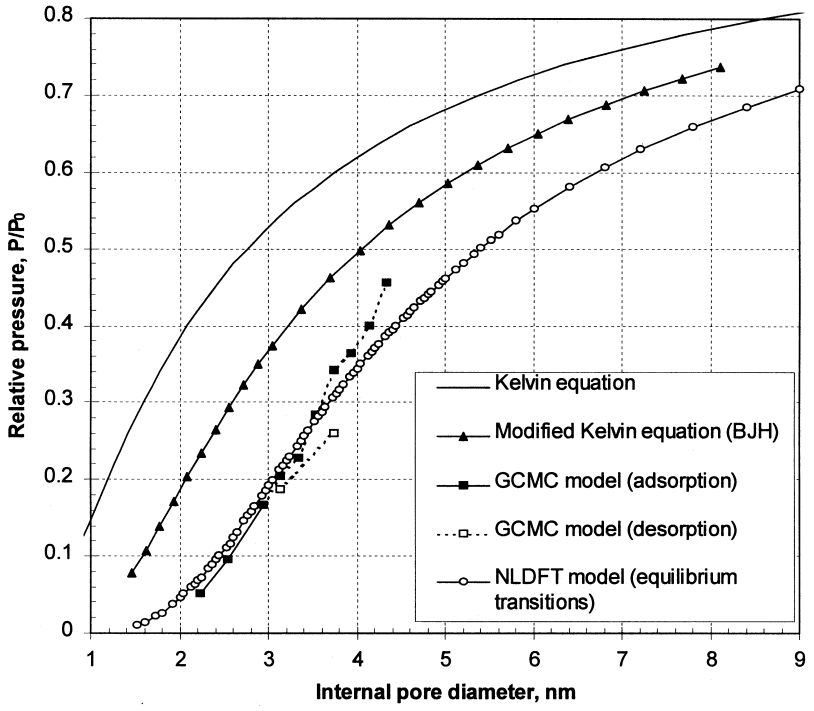

Fig. 3. The pore size dependence of the relative pressure of equilibrium capillary condensation/desorption transition for N_2 in cylindrical pores at 77 K.

the reference samples, the authors [22,23,29,40] have concluded that in nanoporous materials with predominantly cylindrical pore channels, evaporation occurs at the point of equilibrium transition predicted theoretically. This conclusion is consistent with the traditional mechanistic model of evaporation from an open cylindrical pore [101], which assumes that the pore emptying takes place at constant relative pressure and is associated with the displacement of the equilibrium meniscus formed initially at the pore edge. On the contrary, the capillary condensation in an open cylindrical pore involves formation of a meniscus, the process which proceeds via metastable states of adsorbed film, and leads to the hysteresis [101,102]. The hysteresis may not be observed experimentally, or may be substantially narrower than the theoretical predictions because of the fluctuations of the adsorbed film–gas interface and the presence of impurities, which could initiate the system transition toward a state of lower energy.

The relative pressures of the NLDFT equilibrium thermodynamic transitions for nitrogen in cylindrical pores at 77 K are shown in Fig. 3. This curve differs somewhat from that published earlier in [22] because of the new set of the solid–fluid parameters employed for calculations. We also included for comparison the predictions of the Kelvin equation and the modified Kelvin equation used in

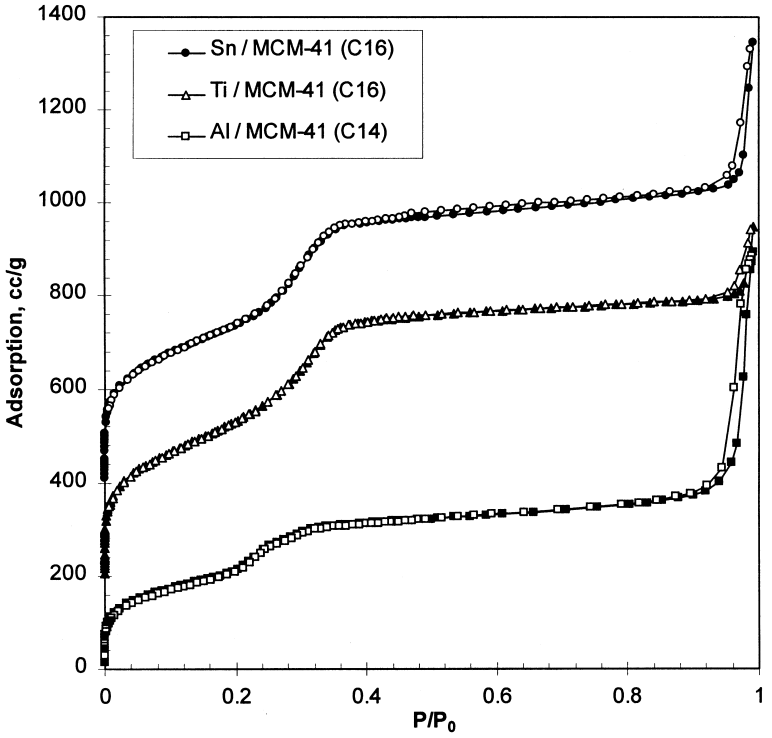

Fig. 4. Nitrogen adsorption isotherms on MCM-41 catalysts. Adsorption, closed points; desorption, open points. The scale is shifted by 200 $cm/^3$ for Ti/MCM-41 and by 400 $cm/^3$ for Sn/MCM-41 sample.

the BJH model. The modified Kelvin equation predicts the transition pressures which are too high in comparison with the NLDFT model, and consequently, the BJH method underestimates the pore size.

It is of interest to compare the NLDFT predictions for the capillary condensation pressure with the results of recent Grand Canonical MC simulations of nitrogen adsorption on MCM-41 [61]. Maddox et al. [61] used a refined model, in which the energetic heterogeneity of the MCM-41 surface has been taken into account by varying a two-dimensional potential of the solid–fluid interactions along the circumference of the cylindrical pore. This approach violates the symmetry of the pore, but it allows an excellent fit to the low-pressure region of the experimental isotherms to be obtained. The predictions of the MC model are also shown in Fig. 3. Note that the pore diameters shown are the internal ones, i.e. we subtracted from the pore diameters reported in Fig. 6 from [61] the diameter of the oxygen atom, 0.265 nm [61]. The comparison indicates that the NLDFT and the MC predictions are very close for pores smaller than the capillary critical pore size in the MC model which is approximately 3 nm [61], i.e. in the region of reversibility of

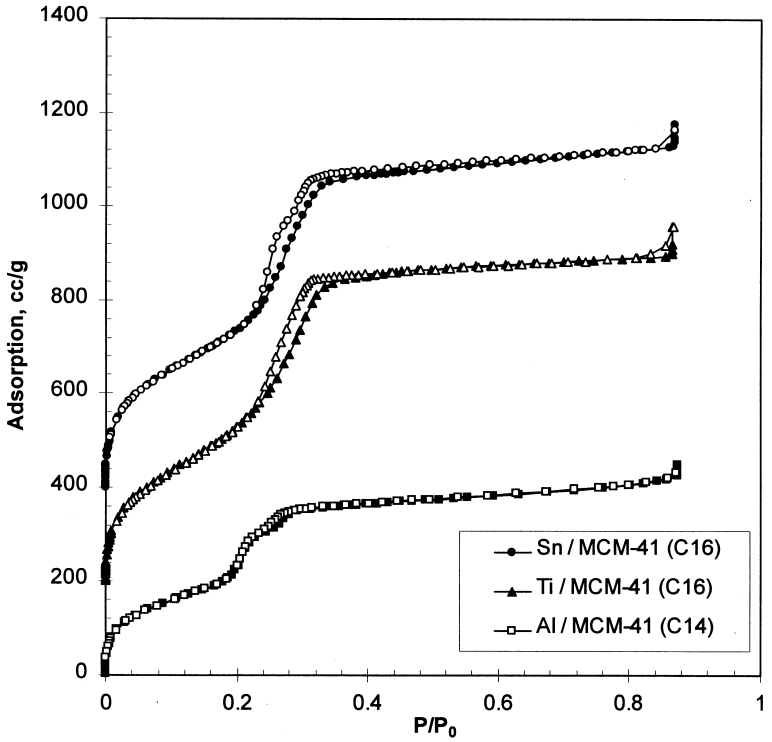

Fig. 5. Argon adsorption isotherms on MCM-41 catalysts. The saturation pressure of the supercooled liquid argon was used. Adsorption, closed points; desorption, open points. The scale is shifted by 200 cm^3/g for Ti/MCM-41 and by 400 cm^3/g for Sn/MCM-41 sample.

the MC adsorption and desorption isotherms. In larger pores, where the MC simulations gave the hysteretic isotherms, the points of the equilibrium thermodynamic transitions were undetermined, and the authors [61] used the adsorption metastable branches of the MC isotherms. These metastable adsorption points are indicated in Fig. 3 with a dashed line. We also plotted the transition pressures determined from the desorption branches of the MC simulations from Fig. 10 of Ref. [61]. The points of the equilibrium thermodynamic transition lie between the points of adsorption and desorption transitions. Therefore, Fig. 3 allows one to believe that the MC equilibrium transition pressures would agree with the NLDFT predictions.

5. Calculation of pore size distributions in nanoporous catalysts

With a set of model isotherms in individual pores, the experimental isotherm can

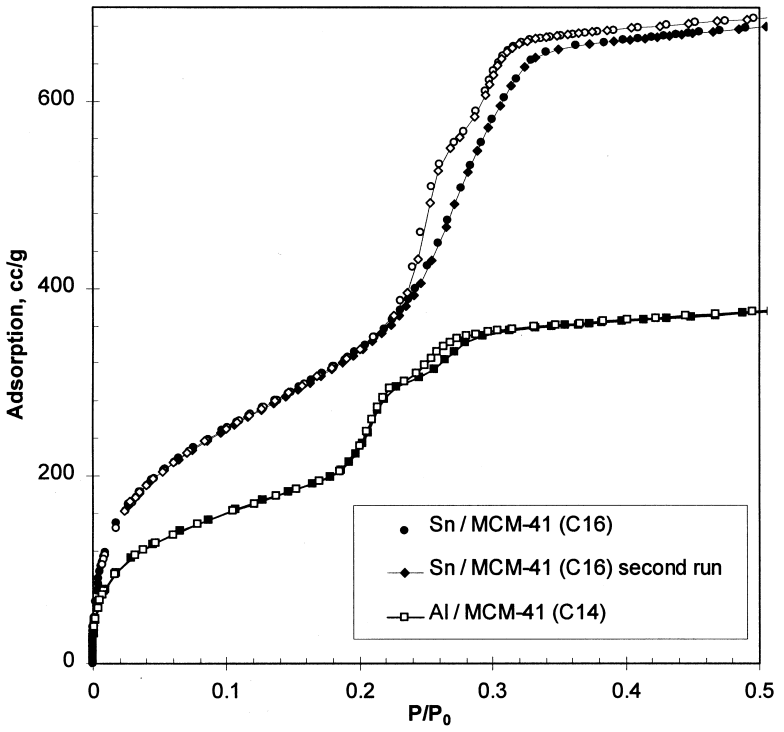

Fig. 6. Argon hysteresis loops on Sn and Al/MCM-41 samples. Adsorption, closed points; desorption, open points. Different symbols for Sn/MCM-41 sample denote different runs.

be described as a superposition of the model isotherms and the pore size distribution:

$$N_{\mathrm{exp}}(P/P_0) = \int_{D_{\mathrm{min}}}^{D_{\mathrm{Lmax}}} \varphi(D_{\mathrm{in}}) N_{\mathrm{V}}(D_{\mathrm{in}}, P/P_0)\, \mathrm{d}D_{\mathrm{in}} \tag{11}$$

where $N_{\mathrm{exp}}(P/P_0)$ is the experimental isotherm, $N_{\mathrm{DFT}}(D_{\mathrm{in}}, P/P_0)$ is the theoretical isotherm in a model pore of size D_{in}, and $\varphi(D_{\mathrm{in}})$ is the pore volume distribution. Solution of the integral Eq. (11) is obtained by solving a corresponding linear least-squares problem [43]. Assuming that an array of open cylindrical pores is a plausible approximation of the pore system in the MCM-41 materials, we are inclined to believe that, in the case of hysteresis, the desorption branch of the experimental isotherm corresponds to the equilibrium transitions in individual pores [22,23]. Therefore, we calculate the pore size distributions from the desorption branches of the experimental isotherms.

As an example of the NLDFT approach, we present below calculations of the pore size distributions of three nanoporous MCM-41 catalysts, containing Al, Ti,

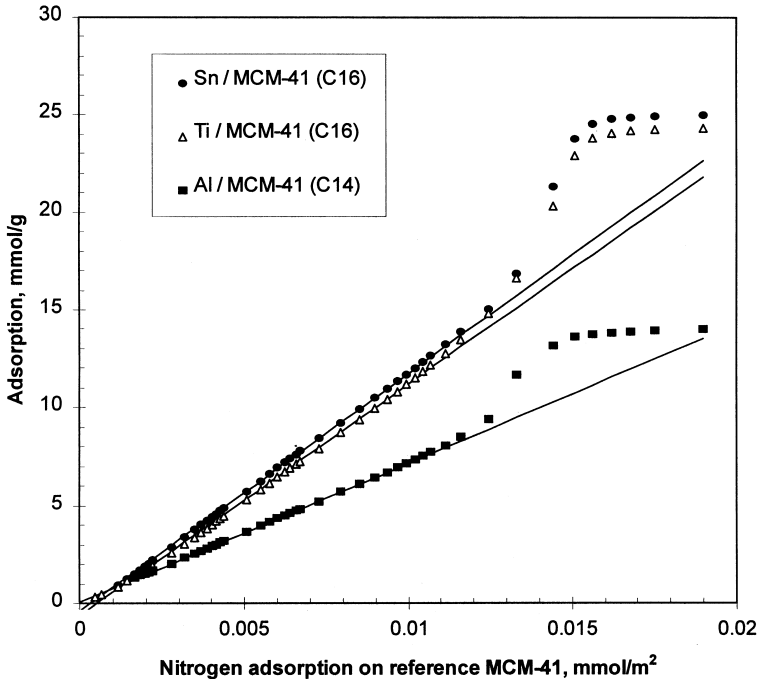

Fig. 7. Nitrogen comparison plots versus isotherm on a reference MCM-41 sample [22].

and Sn. The synthesis procedure will be described elsewhere. The adsorption isotherms of nitrogen and argon were measured at 77 K with the automated volumetric instrument Autosorb-1C (Quantachrome, USA), starting from the relative pressure $P/P_0 \approx 1 \times 10^{-5}$. For Ar at 77 K, the saturation pressure of supercooled liquid Ar was used. Nitrogen isotherms (Fig. 4) are reversible for all samples. The isotherm on Al/MCM-41 exhibits a large uptake at high relative pressures indicating an increased proportion of the secondary macroporous structure to the primary mesoporous structure. A very interesting, and highly unusual feature of the isotherms on the Al/MCM-41 sample is the presence of the second sub-step at the relative pressure $P/P_0 \approx 0.28$. For the Ar isotherm (Fig. 5) this step is accompanied by a small but well-defined hysteresis. A hysteresis loop typical for isotherms in cylindrical pores is observed for the Ar isotherm on the Ti/MCM-41 sample. For the Sn/MCM-41 sample, however, the desorption branch of the Ar hysteresis loop exhibits an unusual sub-step, while the adsorption branch is smooth (Fig. 5). An expanded plot with more details is shown in Fig. 6. We have also performed a second measurement of the Ar isotherm on the Sn/MCM-41 sample using 3.5 longer equilibration time at each point, and have not observed any difference between the two measurements. The hysteresis loops observed for Al and Sn-containing samples are unusual, and clearly indicate that the structure of the metal-containing M41S catalysts can be more complex than the ideal hexagonal

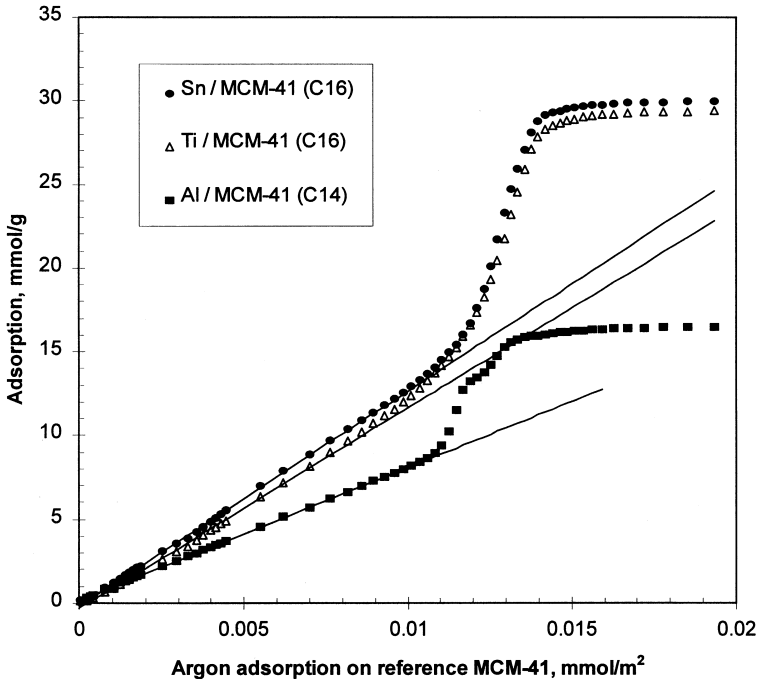

Fig. 8. Argon comparison plots versus isotherm on a reference MCM-41 sample [22].

Table 2
Pore structure parameters of nanoporous catalysts

Sample	a_0 (Å)	Gas	S_{BET} (m^2/g)	S_{cmp} (m^2/g)	V_p (cm^3/g)	$V^{DFT}{}_p$ (cm^3/g)	$S^{DFT}{}_p$ (m^2/g)	$D^{DFT}{}_p$ (Å)	d_{wall} (Å)
Al MCM-41	40.7	N_2	725	708	0.5	0.48	578	32/36	4.7/8.7
		Ar		758		0.44	568	32.5/36	4.7/8.2
Sn MCM-41	42.3	N_2	1193	1212	0.89	0.89	968	36	6.3
		Ar		1279		0.81	935	35.7/39.7	2.5/6.6
Ti MCM-41	n/a	N_2	1189	1179	0.86	0.84	934	37	n/a
		Ar		1194		0.78	884	37	

$a_0 = 2/\sqrt{3}\ d_{100}$ is a distance between pores calculated from XRD data assuming a hexagonal unit cell.
S_{BET} was calculated using the molecular cross-sectional area of N_2, 0.162 nm^2/molecule.
S_{cmp} obtained from the comparison plots.
IV_p is a pore volume determined from N_2 isotherms at $P/P_0 = 0.5$ using the bulk liquid nitrogen density.
V_p^{DFT} and S_p^{DFT} are the pore volume and the pore surface area, respectively, calculated from the NLDFT model.
D_p^{DFT} is the pore diameter taken from the maximum of the PSD curve. For samples with bi-modal PSDs, two values are given.
$d_{wall} = a_0 - D_p^{DFT}$.

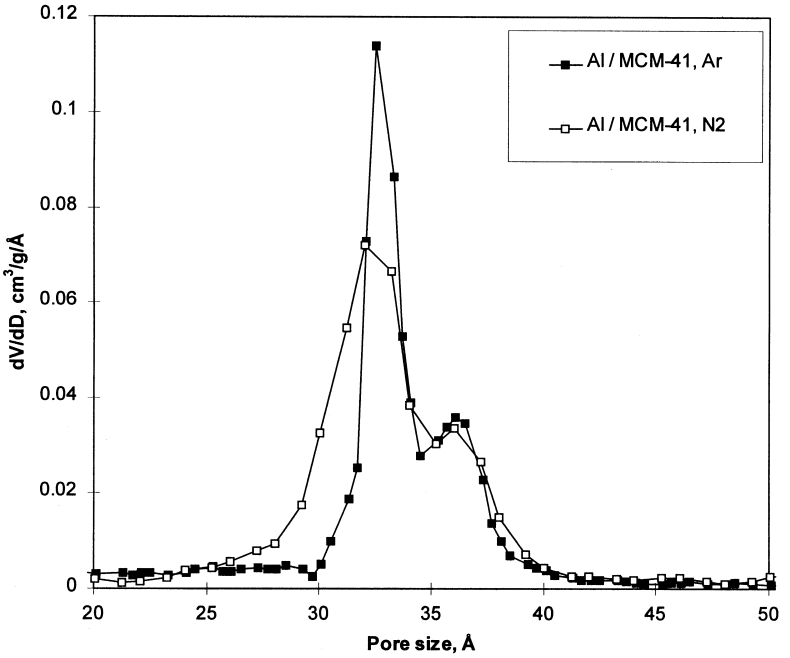

Fig. 9. Pore size distributions of Al/MCM-41 catalyst, calculated from the NLDFT model using desorption isotherms.

array of uniform cylindrical pores of MCM-41. At present, we do not have a clear understanding of the observed sub-steps of the isotherms. As one possible explanation among others, one might consider a structure containing appreciable amounts of other mesophases, such as cubic, or disordered phase. It might also be that pore openings are actually narrower than the mean pore diameter, and thus, pore blocking effects cannot be excluded. The incorporated metals might also be located near pore entrances, rather than in the main channel. It is hardly feasible to account for all of these factors. This example also shows that nitrogen isotherms alone may give little information about all peculiarities of the pore structure, and the use of other adsorbates, e.g. Ar, is advantageous.

In Figs. 7 and 8, we present comparison plots constructed versus nitrogen and argon isotherms on a reference MCM-41 sample [43]. The comparison plots confirm the relative insensitivity of the physical adsorption of nitrogen and argon to the details of the surface chemistry. Figs. 7 and 8 indicate that incorporation of the transition metals practically does not affect the shape of the adsorption isotherm in the mono- and multilayer region. The Ar comparison plots are well-extrapolated back to the origin, indicating the absence of any micropores. Nitrogen comparison plots for Ti and Sn containing samples are also linear with a very small negative intercept of the *y*-axis (Fig. 7). It may be expected that nitrogen should be more sensitive to the surface chemistry than Ar. However, the observed

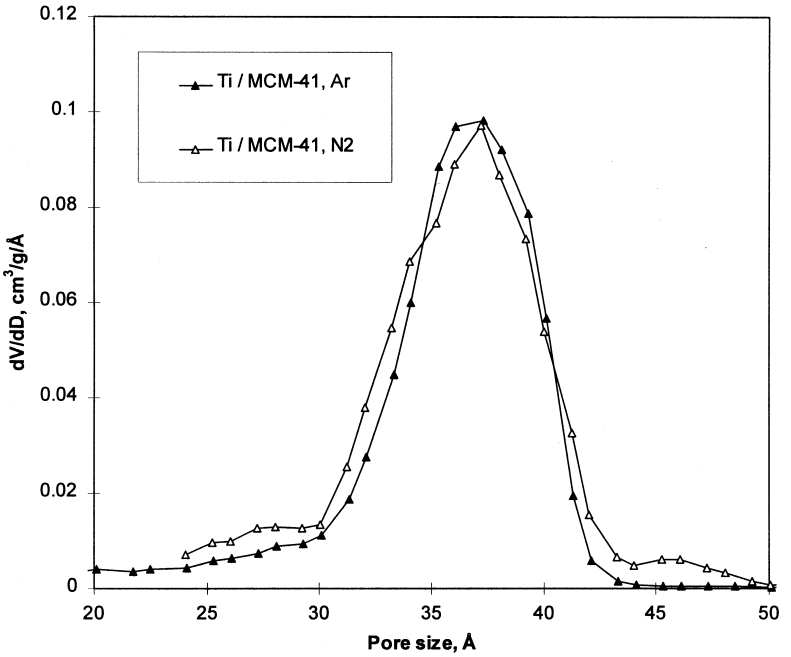

Fig. 10. Pore size distributions of Ti/MCM-41 catalyst, calculated from the NLDFT model using desorption isotherms.

deviations are probably too small to be taken into account, and could be within the experimental errors. More systematic studies on other Ti and Sn modified MCM-41 samples are needed to confirm the observed small deviations. For the purpose of calculation of the pore size distributions, we can conclude that the low-pressure behavior of the nitrogen and argon isotherms on metal-substituted MCM-41 catalysts is the same as the behavior of the isotherms on pure siliceous MCM-41. This is advantageous from the point of view of PSD calculations, because we can use the same model to treat adsorption on pure siliceous, and metal-modified silica surfaces.

Calculated pore size distributions are presented in Figs. 9–11, and the results of the pore structure analysis are summarized in Table 2. We note a good agreement between the results obtained using N_2 and Ar models, especially in the prediction of the pore size. This indicates a consistency of the NLDFT approach. As expected, the pore size distributions of the Al/MCM-41 sample are bi-modal (Fig. 9), because of two steps on both N_2 and Ar isotherms (Figs. 4–6). Pore size distributions of Ti/MCM-41 are unimodal (Fig. 10), and we note a perfect agreement between the results obtained from N_2 and Ar models. For Sn/MCM-41 sample, only Ar desorption isotherm exhibits a second sub-step, thus the PSD obtained from the Ar isotherm is bi-modal, while the nitrogen PSD is unimodal (Fig. 11).

The pore volumes and pore surface areas derived from the NLDFT model agree

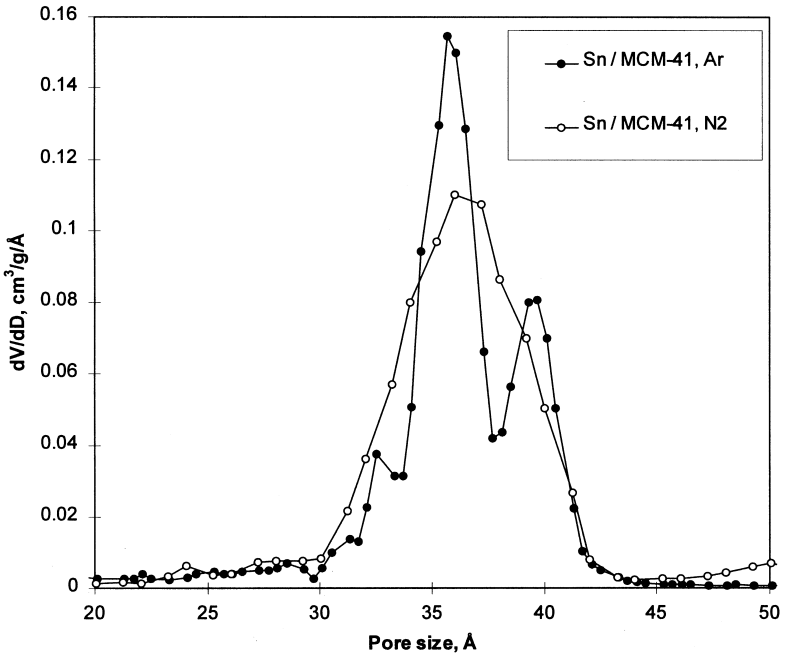

Fig. 11. Pore size distributions of Sn/MCM-41 catalyst, calculated from the NLDFT model using desorption isotherms.

reasonably with the commonly used estimates such as BET and comparison surface areas, and the pore volume calculated using the normal liquid density of the adsorbate (Table 2).

The pore wall thickness has been calculated from available XRD data assuming the hexagonal arrangement of pores. The pore wall thickness of the bi-porous Al/MCM-41 sample was estimated as 0.82–0.87 nm, and the pore wall thickness of Sn/MCM-41 catalysts as 0.63–0.66 nm. These values are in a reasonable agreement with other estimates for the pore wall thickness of MCM-41-like materials (0.7–1 nm) [3,7,25], and much smaller than the results usually obtained using the BJH method (1.5–2.5 nm) [42,43,45].

It should be noted that there is a satisfactory agreement between the NLDFT and the MC models in the prediction of the pore wall thickness in MCM-41. While using the model pore wall composed of three layers of silica (approximately 1 nm), Maddox et al. [61] found that in order to convert the theoretical adsorption into experimental adsorption per unit mass of the sample, the density of the pore wall would have to be reduced by approximately 50%. They concluded that the thickness of pore walls is approximately 0.5–0.6 nm or roughly, two oxygen atoms. Thus, both theoretical models point toward somewhat smaller pore wall thickness in MCM-41 materials than the commonly accepted 1 nm.

6. Conclusions

The non-local density functional theory model has been proven successful in the quantitative description of low-temperature N_2 and Ar adsorption on MCM-41 materials. The predictions of the NLDFT model for the capillary condensation equilibrium transitions in cylindrical pores are in agreement with the desorption branches of the adsorption isotherms on reference MCM-41 samples, and with the results of Monte Carlo simulations.

The NLDFT-based method for calculating the pore size distributions has been applied for the characterization of Ti, Sn and Al-containing MCM-41 catalysts. The low-pressure comparison plots show a good degree of similarity of both N_2 and Ar adsorption on metal-substituted MCM-41 samples to the adsorption on pure silica MCM-41. No evidence of the microporosity has been found. It has been shown, however, that the mesopore structure of the nanoporous catalysts may be quite complex. Unusual sub-steps on the experimental isotherms and corresponding pore size distributions point toward bi-modal structure of Al/MCM-41 and Sn/MCM-41 catalysts. The pore size distributions obtained from the desorption branches of N_2 and Ar isotherms are in satisfactory agreement indicating consistency of the NLDFT model. The results obtained for the pore wall thickness of nanoporous catalysts agree with the expected structure of the samples.

The NLDFT model is recommended for the characterization of nanoporous materials. The desorption branches of Ar isotherms reflect the peculiarities of nonuniform pore structures in more detail than the N_2 isotherms. Therefore, the employment of the desorption Ar isotherms is preferable for pore size distribution calculations.

Acknowledgements

We thank Anke Hagen, Di Wei and Naisheng Yao, whose samples were used in this work. This work was supported, in part, by Grant DE-FG02-88ER13836 from DOE, Office of Basic Energy Sciences, and the TRI/Princeton exploratory research program.

References

[1] C.T. Kresge, M.E. Leonowicz, W.J. Roth, J.C. Vartuli, J.S. Beck, Nature 359 (1992) 710.
[2] J.S. Beck, J.C. Vartuli, W.J. Roth, M.E. Leonowicz, C.T. Kresge, K.D. Schmitt, C.T.-W. Chu, D.H. Olson, E.W. Sheppard, S.B. McCullen, J.B. Higgins, J.L. Schlenker, J. Am. Chem. Soc. 114 (1992) 10834.
[3] A. Monnier, F. Schüth, Q. Huo, D. Kumar, D. Margolese, R.S. Maxwell, G.D. Stucky, M. Krishnamurty, P. Petroff, A. Firouzi, M. Janicke, B.F. Chmelka, Science 261 (1993) 1299.
[4] Q. Huo, D.I. Margolese, U. Ciesla, D.G. Demuth, P. Feng, T.E. Gier, P. Sieger, A. Firouzi, B.F. Chmelka, F. Schüth, G.D. Stucky, Chem. Mater. 6 (1994) 1176.
[5] J.C. Vartuli, K.D. Schmitt, C.T. Kresge, W.J. Roth, M.E. Leonowicz, S.B. McCullen, S.D. Hellring, J.S. Beck, J.L. Schlenker, D.H. Olson, E.W. Sheppard, Chem. Mater. 6 (1994) 2317.

[6] S. Inagaki, Y. Fukushima, K. Kuroda, J. Chem. Soc. Chem. Commun. (1993) 680.
[7] C.-Y. Chen, S.-Q. Xiao, M.E. Davis, Microporous Mater. 4 (1995) 1.
[8] P.T. Tanev, T.J. Pinnavaia, Science 267 (1995) 865.
[9] P.T. Tanev, T.J. Pinnavaia, Chem. Mater. 8 (1996) 2068.
[10] Q. Huo, R. Leon, P.M. Petroff, G.D. Stucky, Science 268 (1995) 1324.
[11] C.-Y. Chen, H.-X. Li, M.E. Davis, Microporous Mater. 2 (1993) 17.
[12] V. Alfredson, M. Keung, A. Monnier, G.D. Stucky, K.K. Unger, F. Schüth, J. Chem. Soc. Chem. Commun. (1994) 921.
[13] N. Coustel, F. Di Renzo, F. Fajula, J. Chem. Soc. Chem. Commun. (1994) 967.
[14] P.T. Tanev, M. Chibwe, T. Pinnavaia, Nature 368 (1994) 321.
[15] O. Franke, J. Rathouský, G. Schulz-Ekloff, J. Stárek, A. Zukal, in: J. Weitkamp, H.G. Karge, H. Pfeifer, W. Hölderich (Eds.), Studies in Surface Science and Catalysis, Vol. 84, Elsevier, Amsterdam, 1994, p. 77.
[16] T. Maschmeyer, F. Rey, G. Sankar, J.M. Thomas, Nature 378 (1995) 159.
[17] T. Blasco, A. Corma, M.T. Navarro, J. Pérez Pariente, J. Catal. 156 (1995) 65.
[18] K.M. Reddy, I. Moudrakovski, A. Sayari, J. Chem. Soc. Chem. Commun. (1994) 1059.
[19] N. Ulagappan, C.N.R. Rao, Chem. Commun. (1996) 1047.
[20] N.K. Raman, M.T. Anderson, C.J. Brinker, Chem. Mater. 8 (1996) 1682.
[21] A. Sayari, in: H. Chon, S.I. Woo, S.-E. Park (Eds.), Recent Advances and New Horizons in Zeolite Science and Technology, Studies in Surface Science and Catalysis, Vol. 102, Elsevier, Amsterdam, 1996, Ch. 1.
[22] P.I. Ravikovitch, S.C. Ó Domhnaill, A.V. Neimark, F. Schüth, K.K. Unger, Langmuir 11 (1995) 4765.
[23] A.V. Neimark, P.I. Ravikovitch, S.C. Ó Domhnaill, F. Schüth, K.K. Unger, in: M.D. LeVan (Ed.), Fundamentals of Adsorption, Kluwer Academic, Boston, MA, 1996, pp. 667–674.
[24] U. Ciesla, M. Grün, T. Isajeva, A.A. Kurganov, A.V. Neimark, P.I. Ravikovitch, S. Schacht, F. Schüth, K.K. Unger, in: T.J. Pinnavaia, M.F. Thorpe, (Eds.), Access in Nanoporous Materials, Plenum Press, New York, 1995, p. 231.
[25] S. Inagaki, Y. Sakamoto, Y. Fukushima, O. Terazaki, Chem. Mater. 8 (1996) 2089.
[26] B.P. Feuston, J.B. Higgins, J. Phys. Chem. 98 (1994) 4459.
[27] S.J. Gregg, K.S.W. Sing, Adsorption, Surface Area and Porosity, Academic Press, New York, 1982.
[28] E.P. Barrett, L.G. Joyner, P.H. Halenda, J. Am. Chem. Soc. 73 (1951) 373.
[29] A.V. Neimark, P.I. Ravikovitch, in: J.M. Drake, J. Klafter, R. Kopelman (Eds.), Dynamics in Small Confining Systems III, MRS, Symposium Proceedings, Vol. 464, 1997, p. 165.
[30] P.J. Branton, P.G. Hall, K.S.W. Sing, J. Chem. Soc. Chem. Commun. (1993) 1257.
[31] O. Franke, G. Schulz-Ekloff, J. Rathouský, J. Stárek, A. Zukal, J. Chem. Soc. Chem. Commun. (1993) 724.
[32] P.J. Branton, P.G. Hall, K.S.W. Sing, H. Reichert, F. Schüth, K.K. Unger, J. Chem. Soc. Faraday Trans. 90 (1994) 2965.
[33] J. Rathouský, A. Zukal, O. Franke, G. Schulz-Ekloff, J. Chem. Soc. Faraday Trans. 90 (1994) 2821.
[34] P.L. Llewellyn, Y. Grillet, F. Schüth, H. Reichert, K.K. Unger, Microporous Mater. 3 (1994) 345.
[35] J. Rathouský, A. Zukal, O. Franke, G. Schulz-Ekloff, J. Chem. Soc. Faraday Trans. 91 (1995) 937.
[36] P.J. Branton, P.G. Hall, M. Treguer, K.S.W. Sing, J. Chem. Soc. Faraday Trans. 91 (1995) 2041.
[37] R. Schmidt, M. Stöcker, E. Hansen, D. Akporiaye, O.H. Ellestad, Microporous Mater. 3 (1995) 443.
[38] P.L. Llewellyn, Y. Grillet, J. Rouquerol, C. Martin, J.-P. Coulomb, Surf. Sci. 352/354 (1996) 468.
[39] H.Y. Zhu, X.S. Zhao, G.Q. Lu, D.D. Do, Langmuir 12 (1996) 6513.
[40] A.V. Neimark, P.I. Ravikovitch, M. Grün, F. Schüth, K.K. Unger, Characterization of Porous Solids IV, Bath, UK, 1996.
[41] M. Kruk, M. Jaroniec, A. Sayari, Microporous Mater. 9 (1997) 173.
[42] M. Kruk, M. Jaroniec, A. Sayari, J. Phys. Chem. B 101 (1997) 583.
[43] P.I. Ravikovitch, D. Wei, W.T. Chueh, G.L. Haller, A.V. Neimark, J. Phys. Chem. B 101 (1997) 3671.
[44] H. Naono, M. Hakuman, T. Shiono, J. Colloid Interf. Sci. 186 (1997) 360.

[45] C.-F. Cheng, W. Zhou, D.H. Park, J. Klinowski, M. Hargreaves, L.F. Gladden, J. Chem. Soc. Faraday Trans. 93 (1997) 359.
[46] J. Horvath, K. Kawazoe, J. Chem. Eng. Jpn. 16 (1983) 470.
[47] A. Corma, V. Fornés, M.T. Navarro, J. Pérez-Pariente, J. Catal. 148 (1994) 569.
[48] A. Saito, H.C. Foley, AIChE J. 37 (1991) 429.
[49] A. Saito, H.C. Foley, Microporous Mater. 3 (1995) 531.
[50] C.J. Guo, in: L. Bonneviot, S. Kaliaguine (Eds.), Zeolites: A Refined Tool for Designing Catalytic Sites, Elsevier, Amsterdam, 1995, p. 165.
[51] R.F. Cracknell, K.E. Gubbins, M. Maddox, D. Nicholson, Acc. Chem. Res. 28 (1995) 281.
[52] N.A. Seaton, J.P.R.B. Walton, N. Quirke, Carbon 27 (1989) 853.
[53] P.N. Aukett, N. Quirke, S. Riddiford, S.R. Tennison, Carbon 30 (1992) 913.
[54] C. Lastoskie, K.E. Gubbins, N. Quirke, J. Phys. Chem. 97 (1993) 4786.
[55] J.P. Olivier, W.B. Conklin, M.v. Szombathely, in: J. Rouquerol, F. Rodríguez-Reinoso, K.S.W. Sing, K.K. Unger (Eds.), Characterization of Porous Solids III, Studies in Surface Science and Catalysis, Vol. 87, Elsevier, Amsterdam, 1994.
[56] J.P. Olivier, J. Porous Mater. 2 (1995) 217.
[57] N. Quirke, S.R.R. Tennison, Carbon 34 (1996) 1281.
[58] V.Yu. Gusev, J.A. O'Brien, N.A. Seaton, Langmuir 13 (1997) 2815.
[59] V.Yu. Gusev, J.A. O'Brien, Langmuir 13 (1997) 2822.
[60] M.W. Maddox, K.E. Gubbins, Int. J. Thermophys. 15 (1994) 1115.
[61] M.W. Maddox, J.P. Olivier, K.E. Gubbins, Langmuir 13 (1997) 1737.
[62] R. Evans, Adv. Phys. 28 (1979) 143.
[63] J.-P. Hansen, I.R. McDonald, Theory of Simple Liquids, Academic Press, London, 1986.
[64] R. Evans, in: D. Henderson (Ed.), Fundamentals of Inhomogeneous Fluids, Marcel Dekker, New York, 1992, Ch. 5.
[65] D.E. Sullivan, Phys. Rev. B 20 (1979) 3991.
[66] P. Tarazona, R. Evans, Mol. Phys. 79 (1983) 4431.
[67] P. Tarazona, Mol. Phys. 52 (1984) 81.
[68] D.J. Lee, M.M. Telo da Gama, K.E. Gubbins, Mol. Phys. 53 (1984) 1113.
[69] P. Tarazona, Phys. Rev. A 31 (1985) 2672.
[70] B.Q. Lu, R. Evans, M.M. Telo da Gama, Mol. Phys. 55 (1985) 1319.
[71] R. Evans, U. Marini Bettolo Marconi, P. Tarazona, J. Chem. Soc. Faraday Trans. 2 (1986) 1763.
[72] B.K. Peterson, J.P.R.B. Walton, K.E. Gubbins, J. Chem. Soc. Faraday Trans. 2 (1986) 1789.
[73] P. Tarazona, U. Marini Bettolo Marconi, R. Evans, Mol. Phys. 60 (1987) 573.
[74] B.K. Peterson, K.E. Gubbins, Mol. Phys. 62 (1987) 215.
[75] B.K. Peterson, K.E. Gubbins, G.S. Heffelfinger, U. Marini Bettolo Marconi, F. van Swol, J. Chem. Phys. 88 (1988) 6487.
[76] P.C. Ball, R. Evans, J. Chem. Phys. 89 (1988) 4412.
[77] P.C. Ball, R. Evans, Langmuir 5 (1989) 714.
[78] T.K. Vanderlick, L.E. Scriven, H.T. Davis, J. Chem. Phys. 90 (1989) 2422.
[79] E. Kierlik, M.L. Rosinberg, Phys. Rev. A 42 (1990) 3382.
[80] E. Kierlik, M.L. Rosinberg, Phys. Rev. A44 (1991) 5025.
[81] B.K. Peterson, G.S. Heffelfinger, K.E. Gubbins, F. van Swol, J. Chem. Phys. 93 (1990) 679.
[82] Z. Tan, K.E. Gubbins, J. Phys. Chem. 96 (1992) 845.
[83] L. Lajtar, S. Sokolowski, J. Chem. Soc. Faraday Trans. 88 (1992) 2545.
[84] P.E. Balbuena, K.E. Gubbins, Fluid Phase Equilibria 76 (1992) 21.
[85] P.B. Balbuena, K.E. Gubbins, Langmuir 9 (1993) 1801.
[86] C. Lastoskie, K.E. Gubbins, N. Quirke, Langmuir 9 (1993) 2693.
[87] S. Sokolowski, J. Fisher, J. Chem. Soc. Faraday Trans. 89 (1993) 789.
[88] P.B. Balbuena, K.E. Gubbins, in: J. Rouquerol, F. Rodríguez-Reinoso, K.S.W. Sing, K.K. Unger (Eds.), Characterization of Porous Solids III, Studies in Surface Science and Catalysis, Vol. 87, Elsevier, Amsterdam, 1994.
[89] S. Jiang, P.B. Balbuena, K.E. Gubbins, J. Phys. Chem. 98 (1994) 2403.
[90] G. Chmiel, A. Patrykiejew, W. Rzysko, S. Sokolowski, Mol. Phys. 83 (1994) 19.

[91] A.V. Neimark, V.Yu. Gusev, J. O'Brien, P.I. Ravikovitch, in: Recent Developments and Future Opportunities in Separations Technology, Proc. AIChE Annual Meeting, Vol. 2, Miami Beach, 1995, p. 17.
[92] P.I. Ravikovitch, A.V. Neimark, S. Schacht, F. Schüth, K.K. Unger, in: Recent Developments and Future Opportunities in Separations Technology, Proc. AIChE Annual Meeting, Vol. 2, Miami Beach, 1995, p. 11.
[93] S.L. Sowers, K.E. Gubbins, in: M.D. LeVan (Ed.), Fundamentals of Adsorption, Kluwer Academic, Boston, MA, 1996, p. 855.
[94] A.V. Neimark, P.I. Ravikovitch, Langmuir 13 (1997) 5148.
[95] N.F. Carnahan, K.E. Starling, J. Chem. Phys. 51 (1969) 635.
[96] J.D. Weeks, D. Chandler, H.C. Andersen, J. Chem. Phys. 54 (1971) 5237.
[97] A.V. Neimark, Langmuir 11 (1995) 4183.
[98] G.J. Tjatjopoulos, D.L. Feke, J.A. Mann, Jr., J. Phys. Chem. 92 (1988) 4006.
[99] J.H. de Boer, B.G. Linsen, Th.J. Osinga, J. Catalysis 4 (1965) 643.
[100] M.M. Dubinin, L.I. Kataeva, V. Ulin, Proc. Acad. Sci. USSR 3 (1977) 510.
[101] D.H. Everett, in: E.A. Flood (Ed.), The Solid–Gas Interface, Vol. 2, Marcel Dekker, New York, 1967, Ch. 36.
[102] G.S. Heffelfinger, F. van Swol, K.E. Gubbins, J. Chem. Phys. 89 (1988) 5202.